Genetic Reduction of Glucose Metabolism Preserves Functional β-Cell Mass in K_{ATP}-Induced Neonatal Diabetes

Zihan Yan,[1] Manuela Fortunato,[1] Zeenat A. Shyr,[1] Amy L. Clark,[2] Matt Fuess,[1] Colin G. Nichols,[3,4] and Maria S. Remedi[1,3,4]

Diabetes 2022;71:1233–1245 | https://doi.org/10.2337/db21-0992

β-Cell failure and loss of β-cell mass are key events in diabetes progression. Although insulin hypersecretion in early stages has been implicated in β-cell exhaustion/failure, loss of β-cell mass still occurs in K_{ATP} gain-of-function (GOF) mouse models of human neonatal diabetes in the absence of insulin secretion. Thus, we hypothesize that hyperglycemia-induced increased β-cell metabolism is responsible for β-cell failure and that reducing glucose metabolism will prevent loss of β-cell mass. To test this, K_{ATP}-GOF mice were crossed with mice carrying β-cell–specific glucokinase haploinsufficiency ($GCK^{+/-}$), to genetically reduce glucose metabolism. As expected, both K_{ATP}-GOF and K_{ATP}-GOF/$GCK^{+/-}$ mice showed lack of glucose-stimulated insulin secretion. However, K_{ATP}-GOF/$GCK^{+/-}$ mice demonstrated markedly reduced blood glucose, delayed diabetes progression, and improved glucose tolerance compared with K_{ATP}-GOF mice. In addition, decreased plasma insulin and content, increased proinsulin, and augmented plasma glucagon observed in K_{ATP}-GOF mice were normalized to control levels in K_{ATP}-GOF/$GCK^{+/-}$ mice. Strikingly, K_{ATP}-GOF/$GCK^{+/-}$ mice demonstrated preserved β-cell mass and identity compared with the marked decrease in β-cell identity and increased dedifferentiation observed in K_{ATP}-GOF mice. Moreover K_{ATP}-GOF/$GCK^{+/-}$ mice demonstrated restoration of body weight and liver and brown/white adipose tissue mass and function and normalization of physical activity and metabolic efficiency compared with K_{ATP}-GOF mice. These results demonstrate that decreasing β-cell glucose signaling can prevent glucotoxicity-induced loss of insulin content and β-cell failure independently of compensatory insulin hypersecretion and β-cell exhaustion.

Failure of pancreatic β-cell function and loss of β-cell mass are key events in the development and progression of multiple forms of diabetes. In type 2 diabetes, an initial increase of insulin secretion followed by loss of β-cell function are early events, while substantial loss of β-cell mass occurs closer to the clinical manifestation (1). In pancreatic β-cells, ATP-sensitive potassium (K_{ATP}) channels play a critical role in linking glucose metabolism to insulin secretion. Accordingly, K_{ATP} gain-of-function (GOF) mutations cause human neonatal diabetes (2,3), and K_{ATP}-GOF polymorphisms are associated with development of type-2 diabetes (4). Recapitulating the features of human neonatal diabetes, transgenic expression of K_{ATP}-GOF mutations in mouse β-cells causes rapid and severe diabetes as a result of suppression of insulin secretion (5–7). As diabetes progresses, islets from K_{ATP}-GOF mice show marked loss of both β-cell mass and identity (8). Decreased β-cell mass and identity has also been demonstrated in multiple animal models of monogenic, type 1, and type 2 diabetes (9) and in pancreata from individuals with diabetes (10–13), suggesting potentially common mechanisms in different forms of diabetes independent of the underlying diabetes etiology.

Glucose phosphorylation by glucokinase (GCK) is normally a rate-limiting step in glucose metabolism and a central regulator of glucose-stimulated insulin secretion

[1]Division of Endocrinology, Metabolism and Lipid Research, Department of Medicine, Washington University School of Medicine, St. Louis, MO
[2]Department of Pediatrics, Washington University School of Medicine, St. Louis, MO
[3]Deparment of Cell Biology and Physiology, Washington University School of Medicine, St. Louis, MO
[4]Center for the Investigation of Membrane Excitability Diseases, Washington University School of Medicine, St. Louis, MO

Corresponding author: Maria S. Remedi, mremedi@wustl.edu

Received 4 November 2021 and accepted 9 March 2022

(GSIS) (14), and absence of GCK is expected to reduce glucose flux in β-cells and as a consequence, decrease insulin secretion and increase blood glucose levels (15). Sustained catalytic activation of β-cell GCK has been proposed as a potential cause of the compensatory increase in glucose sensitivity in early stages of the type 2 diabetes (16,17), but the same overstimulation of β-cell metabolism is also proposed as a culprit in subsequent "exhaustion" and loss of β-cell mass (18–20). We previously demonstrated increased glucose metabolism, as reflected in increased NAD(P)H autofluorescence and mitochondrial depolarization, in islets from K_{ATP}-GOF diabetic mice (21). We hypothesize that chronic hyperglycemia increases β-cell metabolic activity, leading to glucotoxicity-induced β-cell failure, potentially in multiple forms of diabetes, and therefore could be prevented by reducing β-cell glucose metabolism. To test this hypothesis in vivo, we examined the effects of reduced GCK activity on the development of diabetes in K_{ATP}-GOF–induced neonatal diabetic mice crossed with β-cell–specific GCK haploinsufficient mice ($GCK^{+/-}$). We show that double-mutant K_{ATP}-GOF/$GCK^{+/-}$ mice, with deceleration of β-cell glucose metabolism, exhibit markedly slower development of systemic diabetes, with preservation of insulin content and β-cell mass and identity, as well as improved insulin sensitivity and adipose tissue mass and function, compared with K_{ATP}-GOF mice with wild-type GCK. This improvement of glucose homeostasis in neonatal diabetic mice by reduction of hypermetabolism-induced β-cell glucotoxicity raises the possibility that such paradoxical protection may be found in other forms of diabetic glucotoxicity.

RESEARCH DESIGN AND METHODS

Animals

All animal studies were performed in accordance with protocols approved by the institutional animal care and use committee of Washington University. Mice were maintained on a regular chow ad libitum diet and housed in a 12 h light/dark cycle. β-Cell–specific heterozygous GCK knockout ($GCK^{+/-}$) mice (22,23) were crossed with β-cell–specific tamoxifen-inducible K_{ATP}-GOF (Rosa-kir6.2[K185Q,ΔN30] × tamoxifen-inducible $Pdx1^{PB}Cre^{ERTM}$) mice (6) to generate double-transgenic K_{ATP}-GOF/$GCK^{+/-}$ mice. Ten- to 12-week-old K_{ATP}-GOF or K_{ATP}-GOF/$GCK^{+/-}$ mice were injected with five consecutive daily doses of tamoxifen (50 μg/g body weight) to induce K_{ATP}-GOF expression (6). Littermate wild-type, Rosa-kir6.2[K185Q,ΔN30], or $Pdx1^{PB}Cre^{ERTM}$ mice were used as controls since no significant differences were found among genotypes (6,7) and among GCK-deficient $GCK^{+/-}$, $Pdx1^{PB}Cre^{ERTM}/GCK^{+/-}$, or [K185Q,ΔN30]/$GCK^{+/-}$ mice. All controls and $GCK^{+/-}$ mice were injected with the same daily dose of tamoxifen. Approximately equal number of males and females were used for all experiments; males and females were averaged together since no significant sex differences were found in any of the genotypes tested.

Blood Glucose and Plasma Hormone Measurements

Nonfasted and fasted blood glucose were measured by using a Bayer Contour T5 glucometer (Mishiwaka, IN). Whole blood was collected in heparinized tubes with protease inhibitor cocktail (3.6 mg/mL benzamidine hydrochloride, 1 mg/mL aprotinin, 1 mmol/L sitagliptin, and 25 mmol/L EDTA). Plasma insulin was assayed using rat/mouse ELISA kit (Crystal Chem, Elk Grove Village, IL). Plasma hormones (insulin, glucagon, glucagon-like peptide 1 [GLP-1], and leptin) were measured using the Luminex MILLIPLEX Mouse Metabolic Hormone panel at the Immunomonitoring Laboratory, Bursky Center for Human Immunology and Immunotherapy Programs Assay Core (https://chiips.wustl.edu) (24). After a 4 h fast, blood glucose was collected for triglyceride, cholesterol, and free fatty acid (FFA) measurement at the Washington University Diabetes Models Phenotyping Core (https://diabetesresearchcenter.dom.wustl.edu/diabetes-models-phenotyping-core) (25).

Glucose Tolerance Tests and Insulin Tolerance Tests

Glucose tolerance tests (GTTs) and insulin tolerance tests (ITTs) were performed after overnight and 5-h fast, respectively. Blood glucose was measured before (0 min) and after (15, 30, 45, 60, 90, and 120 min) intraperitoneal injection of 1.5 mg/kg dextrose (GTT) or 0.5 units/kg human insulin (ITT) (HI-210; Eli Lilly). Blood was also collected at 0 and 30 min after glucose challenge (GTT) for measurement of insulin secretion as described above. Insulinogenic index (*II*) at 30 min after glucose challenge was calculated as follows (26):
$II_{30min} = 0.0077 \times (\text{insulin}_{30\text{min}} - \text{insulin}_{0\text{min}}\ [\text{pmol/L}]) / (\text{glucose}_{30\text{min}} - \text{glucose}_{0\text{min}}\ [\text{mmol/L}])$.

Islet Isolation and Assessment of Insulin Secretion

For pancreatic islet isolation, ice-cold 0.45 mg/mL collagenase type V buffer (Sigma-Aldrich, St. Louis, MO) (in Hanks' balanced salt solution without Ca^{2+}) was perfused into the bile duct. The pancreas was immediately dissected out and incubated at 37°C for 10–11 min in a water bath for digestion, and islets were washed twice in Hanks' balanced salt solution and then handpicked under a stereo microscope. Islets were incubated overnight in RPMI complete media supplemented with 10% FCS, 100 units/mL penicillin, and 100 μg/mL streptomycin (Thermo Fisher Scientific). For GSIS, islets were preincubated in Krebs-Ringer buffer solution (bicarbonate HEPES) containing 2% BSA and 2.8 mmol/L glucose for 1 h. Islets were then separated into groups of 10 and incubated with either 2 or 20 mmol/L glucose for 1 h, and media were collected for GSIS. Total insulin content was extracted from 10 islets in 0.2 N/80% acid ethanol. Insulin released into the medium and total insulin content were measured using a rat/mouse insulin ELISA kit (Crystal Chem) (25). Total proinsulin content was measured using a rat/mouse proinsulin ELISA kit (Mercodia).

Body Fat and Lean Mass Analysis Using MRI

For measurement of percent body fat and lean mass in awake animals, an EchoMRI instrument (Echo Medical Systems, Houston, TX) at the Washington University Diabetes Phenotyping Core was used, as previously described (25).

Metabolic Measurements

Comprehensive metabolic, behavioral, and physiological variables were determined by using TSE PhenoMaster at the Washington University Diabetes Models Phenotyping Core, as previously described (25). The respiratory exchange rate (RER) was calculated as the ratio between the amount of CO_2 produced in metabolism and the O_2 used. The metabolic efficiency was calculated as the ratio between body weight and food consumption.

Hematoxylin-Eosin Staining and Immunohistochemistry

Mice were sacrificed 50 days after the first dose of tamoxifen. Pancreata, epididymal white adipose tissue (WAT), interscapular brown adipose tissue (BAT), and liver from all groups were fixed in 10% neutral buffered formalin and paraffin embedded for sectioning. Serial sections of 5 μm and hematoxylin-eosin (H-E) staining were performed at the Anatomic/Molecular Pathology Core, Washington University. Immunohistochemistry was performed, as previously described (8), by staining with rabbit anti-insulin (1:100; Cell Signaling Technology), mouse antiglucagon (1:100; Cell Signaling Technology), and aldehyde dehydrogenase 1A3 (Aldh1A3) (5 μg/mL; Abcam) antibodies; distribution was visualized using goat antibody conjugated with Alexa Fluor 488 or Alexa Fluor 594 (Molecular Probes, Eugene, OR) with an EXC-500 fluorescence microscope (Visual Dynamix, Chesterfield, MO).

Measurement of β-Cell Mass and Dedifferentiation

Four to five mice from each genotype were sampled on 5-μm-thick sections 25 μm apart (spanning the whole pancreas) and used for immunohistochemical/β-cell mass and immunohistological/dedifferentiation analysis. At least three pancreatic sections from three to five mice of each genotype were covered systematically by accumulating images from nonoverlapping fields on an inverted EXC-500 fluorescent microscope. For β-cell mass, insulin-positive area was measured using ImageJ (RRID:SCR 003070) and calculated as the product of relative β-cell area to whole pancreatic area and pancreatic weight for each mouse. Dedifferentiation was calculated as the number of $ALDH1A3^+$ cells per islet using ImageJ as previously described (11).

Quantitative PCR Analysis

Islet RNA extraction and quantitative real-time PCR analysis were performed as previously described (27). Primers for β-cell identity markers Ins1, NKX6.1, and Pdx1 were previously described (8). Assays for uncoupling protein 1 (UCP-1), peroxisomal proliferator–activated receptor γ (PPARγ), and PPARα genes in BAT; adiponectin, CD36, PPARγ, and leptin in WAT (28); and PPARα/γ, carnitine palmitoyltransferase 1 α (CPT1α), fatty acid synthase (FAS), adipose triglyceride lipase (AGTL), and hormone-sensitive lipase (HSL) in the liver (29) were performed in duplicate and normalized to ribosomal protein mL32 mRNA.

Western Blot Analysis

Fifteen micrograms of total protein lysate were loaded per lane. Blots were incubated overnight with the following antibodies: β-actin (1:1,000; EMD Millipore, St. Louis, MO), thioredoxin-interacting protein (TXNIP) (1:1,000; MBL International, Woburn, MA), and sXBP1 (1:1,000; Santa Cruz Biotechnology, Dallas, TX). Blots were washed and probed with RDye infrared fluorescent dye-labeled red or green secondary antibody conjugates (1:10,000; LI-COR Biosciences). Fluorescence intensity was quantified by Image Studio Lite (LI-COR Biosciences).

Measurement of Liver Triglyceride Content

Total triglycerides were determined by homogenizing 20–30 mg fresh weight liver tissue in 1.5 mL of chloroform:methanol (2:1 v/v). Samples were centrifuged at 12,000 rpm for 10 min at 4°C. An aliquot of 20 μL was evaporated, and triglyceride content was determined by adding 100 μL of reagent after 30 min incubation at room temperature. Measurement of liver triglyceride content was performed at the Washington University Diabetes Models Phenotyping Core.

Statistical Methods

Data are expressed as mean ± SEM. Statistical differences between two groups were determined using Student *t* test and among several groups using ANOVA and post hoc Turkey test for multiple comparisons. Statistical analyses were performed using GraphPad Prism version 8.0 software (GraphPad Software, La Jolla, CA). The threshold of significance was set at $P < 0.05$. Nonsignificant differences are not shown. For Fig. 1, we used lowercase letters in some panels to indicate significance differences of $P < 0.05$ between groups, with the same letter indicating no significant difference.

Data and Resource Availability

The data sets generated and/or analyzed during the current study are available in the figshare repository (https://figshare.com/s/1ec45fbad2f1af649e9b).

RESULTS

Delayed Diabetes Progression and Improved Glucose Tolerance in K_{ATP}-GOF Mice Carrying GCK Haploinsufficiency in β-Cells

The β-cell–specific GCK haploinsufficient mouse ($GCK^{+/-}$) models maturity-onset diabetes of the young 2, a form of monogenic diabetes caused by heterozygous inactivating mutations in the *GCK* gene (22). As a result of decreased β-cell glucose metabolism, individuals with maturity-onset

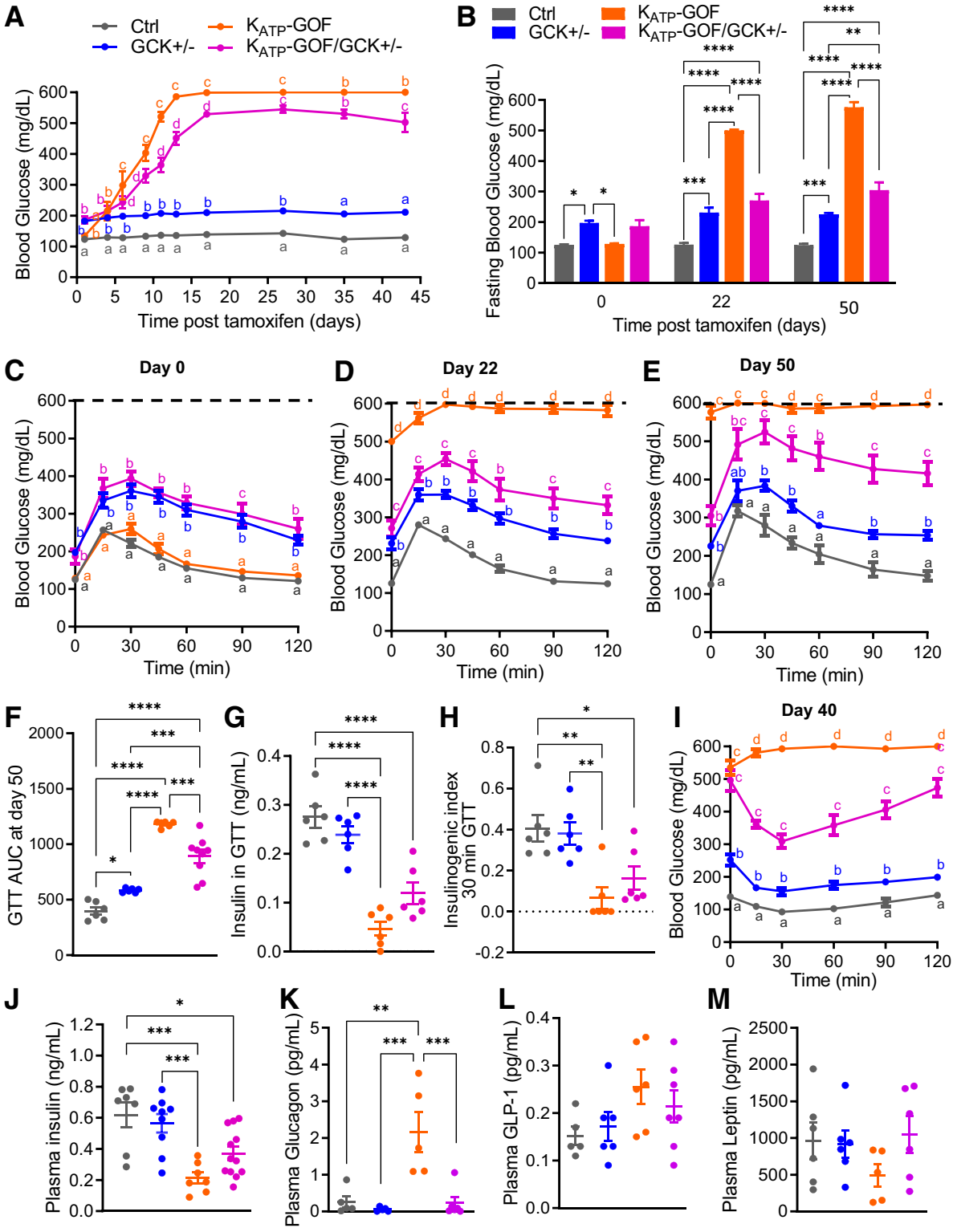

Figure 1—Blood glucose is reduced in K_{ATP}-GOF diabetic mice with reduced β-cell glucokinase. *A*: Nonfasted blood glucose over time in K_{ATP}-GOF mice after tamoxifen induction of transgene expression (n = 9–18 mice/group). *B*: Fasting blood glucose levels at day 0, 22, and 50 after tamoxifen induction (n = 6–9 mice/group). *C–F*: GTT performed at day 0 and at days 22 (n = 4–9 mice/group) and 50 after tamoxifen induction (dashed lines indicate the limit of the detection of the glucose meter) and area under the curve (AUC) (n = 6–9 mice/group). *G* and *H*: Change (Δ) in insulin secretion at 30 min after glucose challenge over fasting (0 min) and *II* during GTT at day 50 after tamoxifen induction (n = 6 mice/group). *I*: ITT performed in mice 40 days after tamoxifen induction. *J–M*: Plasma insulin (n = 8–12 mice/group), glucagon (n = 5 mice/group), GLP-1, and leptin (n = 5–7 mice/group) at day 40 after tamoxifen induction. Data are mean ± SEM. *$P < 0.05$, **$P < 0.01$, ***$P < 0.001$, ****$P < 0.0001$. Nonsignificant differences are not shown. For panels *A*, *C*, *D*, *E*, and *H*, lowercase letters are used to indicate significant differences of $P < 0.05$ between groups. The same letters indicate no significant difference. Ctrl, control.

diabetes of the young 2 and $GCK^{+/-}$ mice show mild, nonprogressive hyperglycemia and do not normally require antidiabetic therapy. As predicted (22,23), both $GCK^{+/-}$ and noninduced K_{ATP}-GOF/$GCK^{+/-}$ mice demonstrated mildly elevated fed and fasting blood glucose levels (Fig. 1*A* and *B*) and slightly impaired glucose tolerance (Fig. 1*C*), while wild-type and noninduced K_{ATP}-GOF mice showed normal blood glucose (Fig. 1*A* and *B*) and glucose tolerance (Fig. 1*C*). After tamoxifen induction of the K_{ATP}-GOF transgene, both K_{ATP}-GOF and K_{ATP}-GOF/$GCK^{+/-}$ mice became progressively diabetic because of K_{ATP} overactivity–induced suppression of GSIS, but the progression is strikingly slowed in the latter (Fig. 1*A* and *B*). At day 22 after tamoxifen induction, K_{ATP}-GOF mice showed remarkably high fasting blood glucose and severely impaired glucose tolerance, but K_{ATP}-GOF/$GCK^{+/-}$ mice were only minimally worse than before induction (Fig. 1*D*). Improved glucose tolerance persisted, with a significantly lower area under the curve (Fig. 1*F*), in K_{ATP}-GOF/$GCK^{+/-}$ compared with K_{ATP}-GOF mice at day 50 (Fig. 1*E*). Lack of increase in blood glucose in severely diabetic K_{ATP}-GOF mice after glucose challenge might be explained by the limit of detection of the glucose meter (values >600 mg/dL considered maximum as denoted by the dashed lines in Fig. 1*C–E*); therefore, glucose tolerance in K_{ATP}-GOF mice may be underestimated. Change in plasma insulin ($insulin_{30\ min}$ − $insulin_{0\ min}$ during GTT) and *II* were higher in K_{ATP}-GOF/$GCK^{+/-}$ mice than in K_{ATP}-GOF mice but did not reach significance (Fig. 1*G* and *H*). At day 40 after tamoxifen induction, random plasma insulin levels were also significantly reduced in both K_{ATP}-GOF and K_{ATP}-GOF/$GCK^{+/-}$ mice compared with controls and not significantly different between them (Fig. 1*J*), reflecting a markedly better insulin sensitivity in K_{ATP}-GOF/$GCK^{+/-}$ mice (Fig. 1*I*). Plasma glucagon, which was significantly increased in K_{ATP}-GOF mice, dropped to normal levels in K_{ATP}-GOF/$GCK^{+/-}$ mice (Fig. 1*K*), and although GLP-1 levels did not change (Fig. 1*L*), leptin levels increased (Fig. 1*M*) in K_{ATP}-GOF/$GCK^{+/-}$ mice with respect to K_{ATP}-GOF mice.

Improved Insulin Content and Reduced Proinsulin and Proinsulin-to-Insulin Ratio in K_{ATP}-GOF/$GCK^{+/-}$ Mice

Plasma lipids, such as triglycerides, cholesterol, and FFAs, were essentially normal in all groups, except for lower FFA levels that were detected in $GCK^{+/-}$ mice (Fig. 2*A*). H-E–stained pancreatic sections revealed disruption of islet architecture only in K_{ATP}-GOF mice (Fig. 2*B*), and immunostaining indicated more insulin and less glucagon in K_{ATP}-GOF/$GCK^{+/-}$ mice compared with K_{ATP}-GOF, which showed a marked decrease in insulin, and infiltration of α-cells into the core of the islet (Fig. 2*C*). These results correlated with the increased plasma glucagon and decreased insulin observed in K_{ATP}-GOF mice but were normal in K_{ATP}-GOF/$GCK^{+/-}$ mice (Fig. 1*I* and *J*). Decreased insulin content in K_{ATP}-GOF islets (Fig. 2*D*) was accompanied by increased proinsulin content and proinsulin-to-insulin ratio (Fig. 2*E* and *F*). Both were normalized in K_{ATP}-GOF/$GCK^{+/-}$ islets (Fig. 2*D–F*), but as predicted, GSIS was reduced in $GCK^{+/-}$, and markedly so in K_{ATP}-GOF and K_{ATP}-GOF/$GCK^{+/-}$ islets, with respect to control islets (Fig. 2*G*).

Islet β-Cell Identity Is Preserved in K_{ATP}-GOF/$GCK^{+/-}$ Mice

While Ins1, NKX6.1, and Pdx1 markers of mature β-cell identity were all significantly decreased in K_{ATP}-GOF islets compared with control and $GCK^{+/-}$ islets, they were partially restored and not significantly different from controls in K_{ATP}-GOF/$GCK^{+/-}$ islets (Fig. 2*H*). Since the progenitor cell marker ALDH1A3 is enriched in dedifferentiated islet endocrine cells from mice and humans with diabetes (11,30), we measured this in islets from the four genotypes. While K_{ATP}-GOF islets showed a significant increase in $ALDH1A3^{+}$ cells (Fig. 2*I*), K_{ATP}-GOF/$GCK^{+/-}$ islets demonstrated a similar number of dedifferentiated cells to control and $GCK^{+/-}$ islets (Fig. 2*I*). TXNIP, which induces β-cell stress by inhibiting thioredoxin, was significantly increased in both K_{ATP}-GOF and K_{ATP}-GOF/$GCK^{+/-}$ islets, suggesting that the markedly high glucose in both models still causes oxidative stress and not mitigated by $GCK^{+/-}$ haploinsufficiency (Fig. 2*J*).

K_{ATP}-GOF/$GCK^{+/-}$ Mice Showed Restored Metabolic Efficiency and Fat Mass

While K_{ATP}-GOF mice demonstrated a significant reduction in body weight by day 40 after tamoxifen induction (6), K_{ATP}-GOF/$GCK^{+/-}$ mice maintained similar weight to control and $GCK^{+/-}$ mice (Fig. 3*A*). MRI assessments of body composition showed no differences in lean mass among the four groups but a significant reduction in fat mass only in K_{ATP}-GOF mice (Fig. 3*B*). Metabolic cage measurements demonstrated a significant increase in food intake in K_{ATP}-GOF mice but normal food intake in K_{ATP}-GOF/$GCK^{+/-}$ (Fig. 3*C*). The RER was not significantly different among the four groups (Fig. 3*D*). Both physical activity and metabolic efficiency were reduced in K_{ATP}-GOF mice, but both were normalized in K_{ATP}-GOF/$GCK^{+/-}$ mice (Fig. 3*E* and *F*).

WAT and BAT Loss in K_{ATP}-GOF Mice Is Restored in K_{ATP}-GOF/$GCK^{+/-}$ Mice

Correlating with fat mass (Fig. 3*A*), both epididymal WAT and interscapular BAT weights were reduced in K_{ATP}-GOF mice but were normal in K_{ATP}-GOF/$GCK^{+/-}$ mice (Fig. 4*A* and *B*). H-E–stained WAT sections showed a slightly reduced adipocyte size and disrupted architecture in K_{ATP}-GOF but a normal size in K_{ATP}-GOF/$GCK^{+/-}$ mice (Fig. 4*C*). BAT staining demonstrated a heterogeneous mixture of large adipocytes containing large vacuoles and small adipocytes in K_{ATP}-GOF mice but normal adipocyte size in K_{ATP}-GOF/$GCK^{+/-}$ mice (Fig. 4*E*). Adiponectin, CD36, leptin, and PPARγ were all markedly reduced in K_{ATP}-GOF WAT but restored to normal levels in K_{ATP}-GOF/$GCK^{+/-}$ (Fig. 4*D*). Because of a lack of insulin and loss of BAT mass in K_{ATP}-GOF mice, UCP-1 would be predicted to increase to maintain thermal homeostasis. However, UCP-1 message

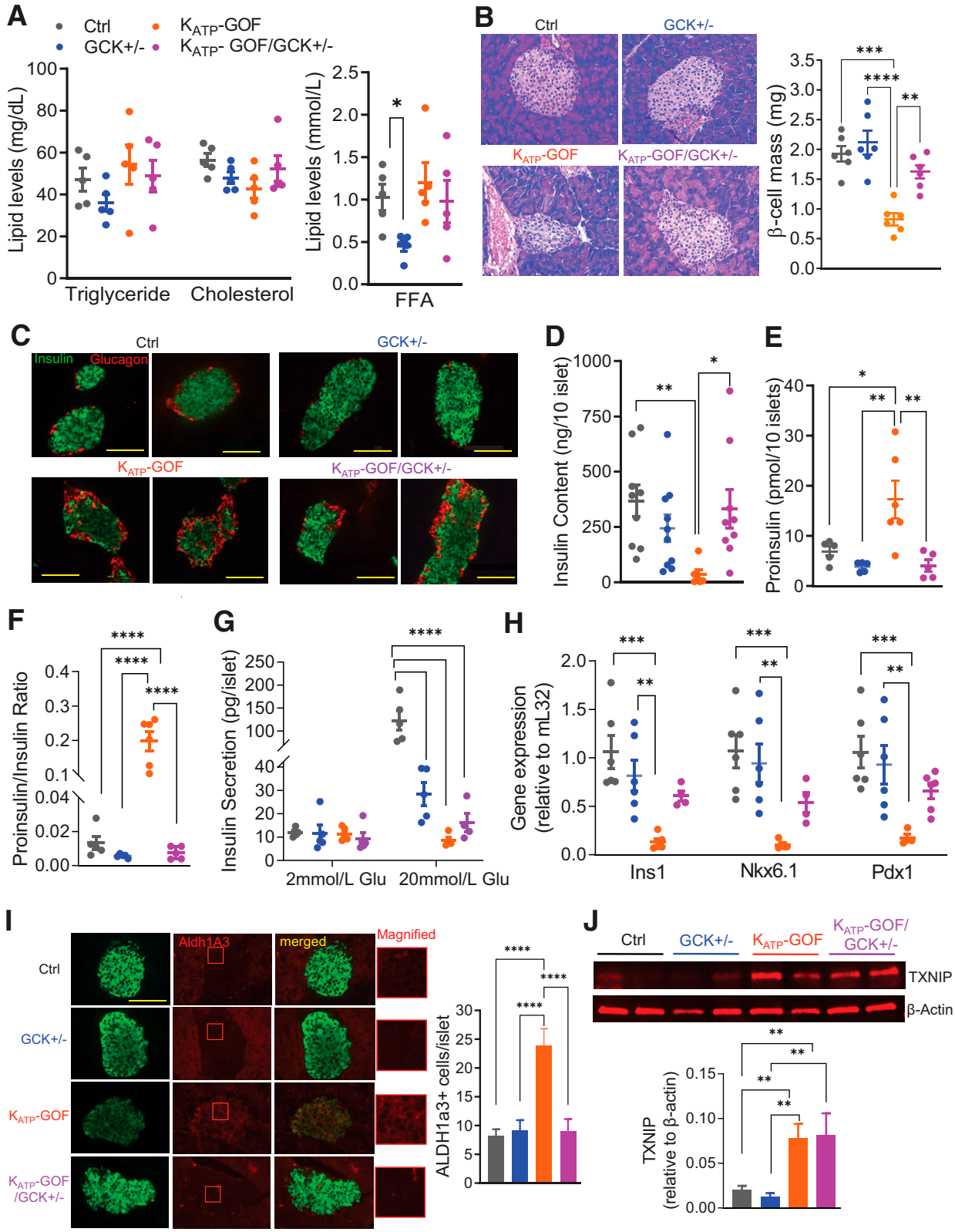

Figure 2—Plasma hormones and lipid levels and cellular stress markers. *A*: Plasma triglyceride, cholesterol (left), and FFAs (right) at day 45 after tamoxifen induction ($n = 5$ mice/group). *B* and *C*: Representative images for *H-E* staining (left) and β-cell mass (right), and insulin (green) and glucagon (red) staining in pancreata at day 45 (scale bars 100 μm, $n = 5$ mice/group). *D*: Total insulin content in islets at day 45 ($n = 6$–10 mice/group). *E* and *F*: Total proinsulin content and proinsulin-to-insulin ratio in islets at day 45 ($n = 5$–6 mice/group). *G*: GSIS at basal (2 mmol/L) and high (20 mmol/L) glucose in islets at day 45 ($n = 5$ mice/group). *H*: Quantitative real-time PCR analysis of Ins1, NKX6.1, and Pdx1 for islets ($n = 4$–6 mice/group). *I*: Representative images for insulin (green), ALDH1A3 (red) (magnified on right), and merged staining on pancreatic sections from all genotype mice, with quantification of ALDH1A31 cells per islet (scale bar 100 μm,

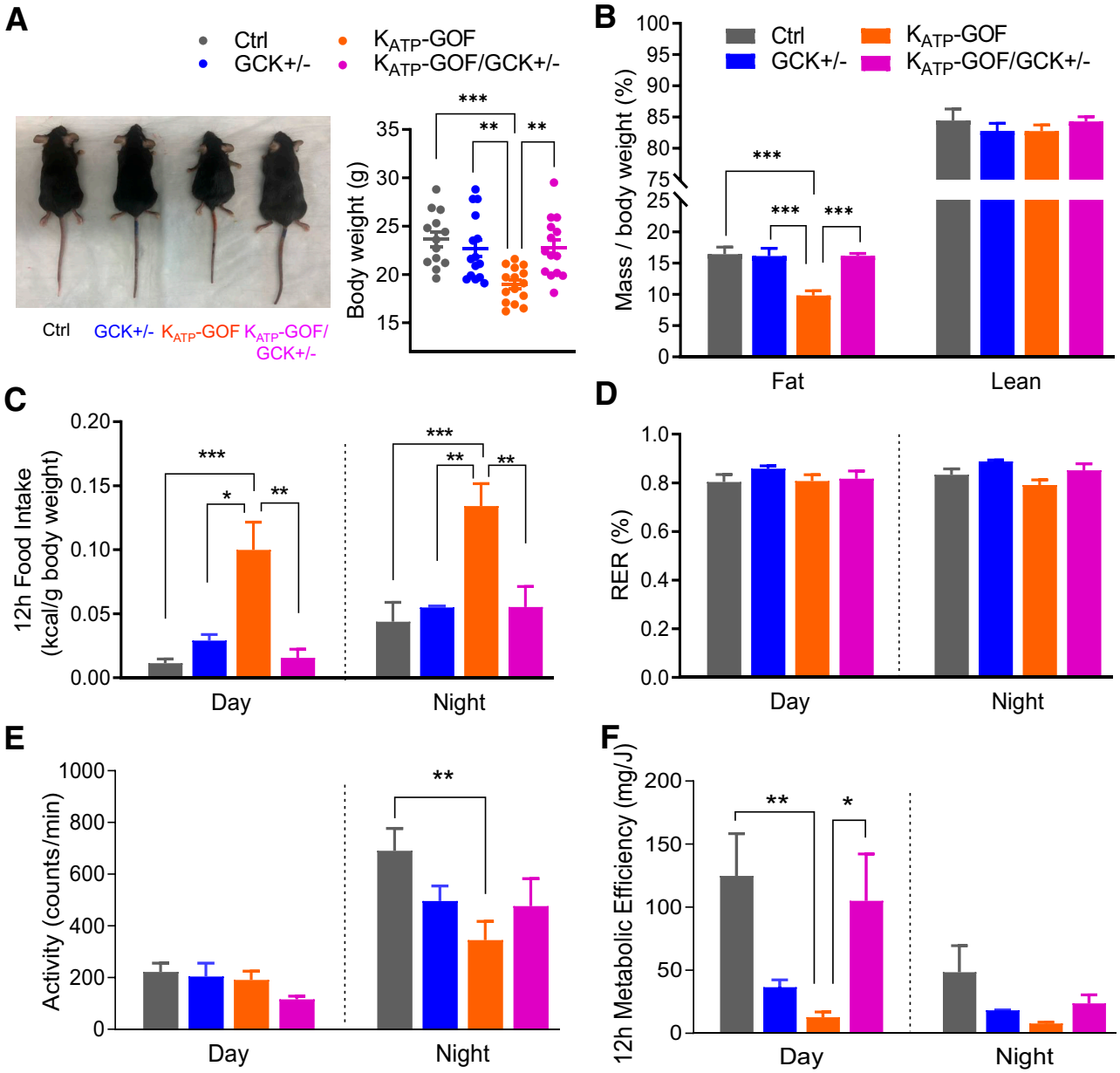

Figure 3—Metabolic phenotyping is improved in K_{ATP}-GOF mice with reduced GCK. *A*: Representative images of mice and quantification of body weight at day 40 after tamoxifen induction (n = 13–15 mice/group). *B*: Fat and lean mass over body weight (n = 5–9 mice/group). *C–F*: Metabolic analysis of food intake in 12 h, RER, physical activity/movement, and metabolic efficiency in 12 h (n = 3–5 mice/group). Data are mean ± SEM. *$P < 0.05$, **$P < 0.01$, ***$P < 0.001$. Nonsignificant differences are not shown. Ctrl, control.

was decreased in these mice (Fig. 4*F*) and normalized in K_{ATP}-GOF/$GCK^{+/-}$ mice. PPARγ and PPARα messages were not significantly different between groups (Fig. 4*F*).

Liver Architecture and Function Are Improved in K_{ATP}-GOF/$GCK^{+/-}$ Mice

Both K_{ATP}-GOF and K_{ATP}-GOF/$GCK^{+/-}$ mice showed significantly increased liver weight with respect to control and $GCK^{+/-}$ mice, and K_{ATP}-GOF livers were heavier than K_{ATP}-GOF/$GCK^{+/-}$ livers (Fig. 5*A*). H-E staining demonstrated altered liver architecture with hepatocytes containing large lipid droplets only in K_{ATP}-GOF mice (Fig. 5*B*), with similar liver architecture and hepatocyte size in K_{ATP}-GOF/$GCK^{+/-}$ relative to those in control and $GCK^{+/-}$ mice (Fig. 5*B*). While triglyceride content significantly increased in livers of K_{ATP}-GOF mice, it was reduced in livers of K_{ATP}-GOF/$GCK^{+/-}$ mice (Fig. 5*C*).

magnified box is 30x30 μm; n = 5 mice/group at day 45). *J*: Representative Western blot and quantitative analysis for islets for TXNIP at day 40 (n = 6–8 mice/group). Data are mean ± SEM. *$P < 0.05$, **$P < 0.01$, ***$P < 0.001$, ****$P < 0.0001$. Nonsignificant differences are not shown. Ctrl, control.

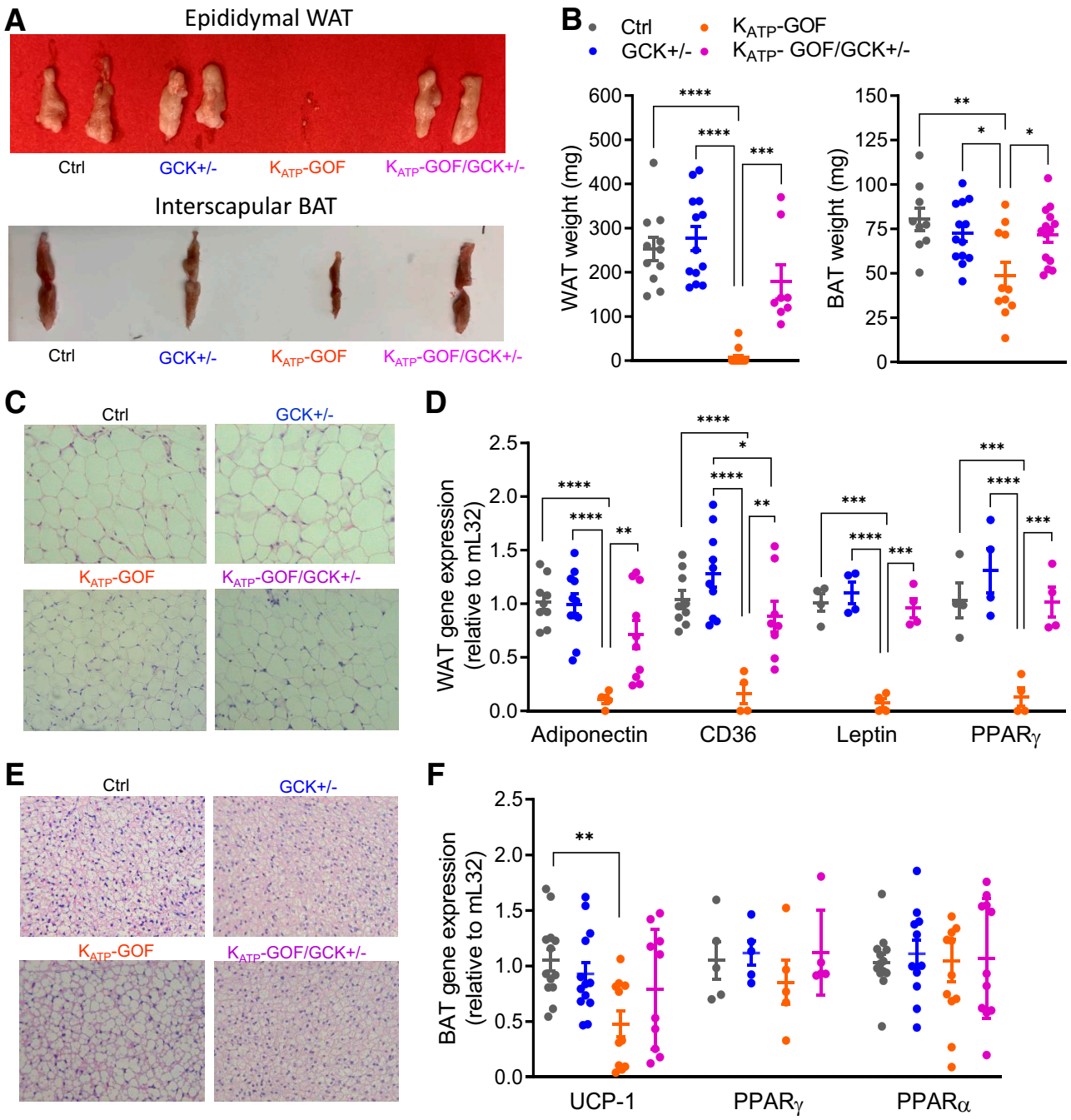

Figure 4—Adipose tissue mass and function are improved in diabetic mice with reduced β-cell GCK. *A*: Representative images of epididymal/gonadal WAT and interscapular BAT. *B*: Quantification epididymal WAT and interscapular BAT (n = 8–15 mice/group). *C* and *E*: Representative images of paraffin sections of H-E–stained WAT and BAT. *D* and *F*: Quantitative real-time PCR analysis of adiponectin, CD36, leptin, and PPARγ for WAT or UCP-1, PPARγ, and PPARα for BAT (n = 4–13 mice/group). Data are mean ± SEM. *$P < 0.05$, **$P < 0.01$, ***$P < 0.001$, ****$P < 0.0001$. Nonsignificant differences are not shown. Ctrl, control.

There were no changes in PPARα, PPARγ, and CPT1α between groups (Fig. 5*D*). FAS, ATGL, and HSL were all reduced only in livers of K_{ATP}-GOF mice (Fig. 5*D*) but normal in K_{ATP}-GOF/GCK$^{+/-}$ mice, suggesting impaired lipolysis in K_{ATP}-GOF but improved in K_{ATP}-GOF/GCK$^{+/-}$ with GCK$^{+/-}$ haploinsufficiency in β-cells.

DISCUSSION

Decreased Glucose-Metabolism as a β-Cell–Protective Mechanism in Glucotoxicity

Progressive deterioration in β-cell function and loss of β-cell mass are common findings in various forms of diabetes (1). We previously demonstrated that chronic

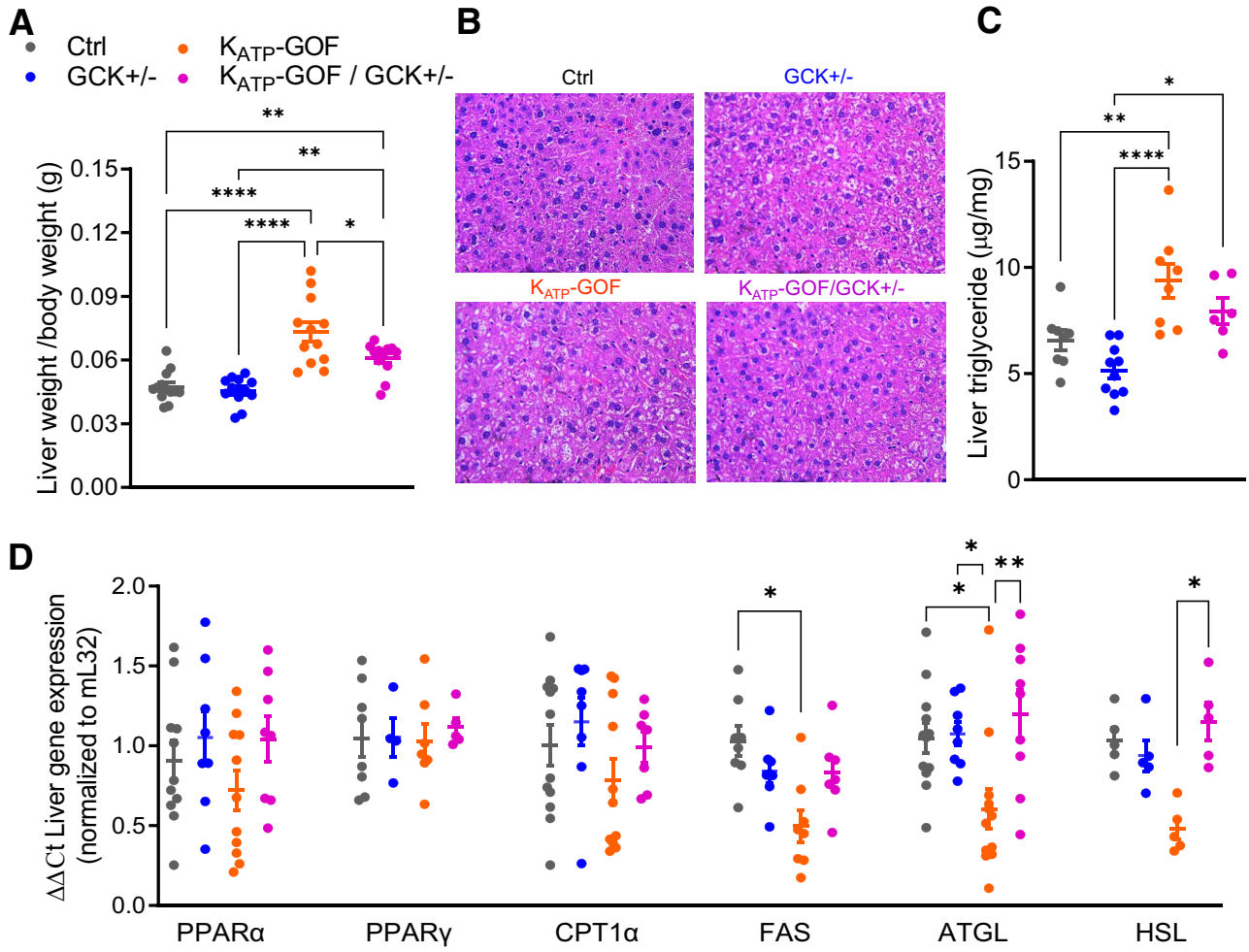

Figure 5—Liver function is improved in diabetic mice with reduced β-cell GCK. *A*: Liver weight/body weight (g) at day 45 after tamoxifen induction (n = 12 mice/group). *B*: Representative images of liver paraffin sections stained with H-E at day 45 after tamoxifen induction. *C*: Liver triglyceride content (n = 8–10 mice/group). *D*: Quantitative real-time PCR analysis for genes involved in β-oxidation (PPARα, PPARγ, and CPT1α), lipogenesis (FAS), and lipolysis (ATGL and HSL) (n = 4–12 mice/group). Data are mean ± SEM. *$P < 0.05$, **$P < 0.01$, ****$P < 0.0001$. Nonsignificant differences are not shown. Ctrl, control.

hyperglycemia gradually leads to a marked loss of insulin content in K_{ATP}-GOF mice (6), changes that were due to loss of β-cell identity rather than to cell death (8), paralleling findings in other rodent models of diabetes of various etiologies (18,31,32). In K_{ATP}-GOF mice, we showed that the loss of insulin content and β-cell identity could be prevented or even reversed by normalization of blood glucose with antidiabetic sulfonylureas or with exogenous insulin treatment (7,8,32) or by feeding with a high-fat diet (25).

There has been much interest in the notion that β-cells become exhausted as a result of the excess demands of secretion induced by hyperglycemia in the diabetic state and that β-cell "rest" through exogenous insulin treatment permits restoration of β-cell function in individuals with type 2 diabetes (33–37). However, our finding that loss of insulin content and β-cell identity occurs in β-cells that are intrinsically inexcitable, and are therefore chronically low in $[Ca^{2+}]_i$ and do not secrete insulin in response to glucose (6,21), indicates that this is not exhaustion due to the demands of excitation or insulin secretion. Instead, somewhere upstream in the pathway from glucose elevation to excitation and secretion must be affected. Increased NAD(P)H autofluorescence and mitochondrial membrane potential in K_{ATP}-GOF mice (21) suggest that augmented β-cell glucose metabolism may be the driving factor in loss of β-cell insulin content in this, and potentially other, diabetic states. This is consistent with the demonstration that metabolism increases when insulin secretion cannot take place and that both increased glycolytic flux and membrane depolarization are necessary for β-cell proliferation (38) and with loss of β-cell mass and apoptosis if proliferation cannot occur. Thus, we suggest that it is rest from hyperstimulation of metabolism, rather than rest from hyperexcitability and secretion, that permits β-cell recovery of insulin content/function in K_{ATP}-GOF mice (27,39).

In the current study we have directly tested the above hypothesis by genetic reduction of glucose metabolism in

K_{ATP}-GOF mice that are also haplodeficient for GCK. Consistent with this hypothesis, K_{ATP}-GOF mice with GCK haploinsufficiency, and thus reduced glucose metabolism (K_{ATP}-GOF/GCK$^{+/-}$), showed delayed diabetes progression, reduced β-cell glucotoxicity, and preserved insulin content and β-cell mass and identity, even though they were still hyperglycemic because of K_{ATP} being permanently "on" and insulin secretion therefore being chronically suppressed. Reduction of GCK activity by D-mannoheptulose (a GCK inhibitor) in newly diabetic *db/db* mouse islets restored glucose sensing and pulsatility of insulin secretion (40). Consistent with previous findings in K_{ATP}-GOF (6) and in GCK (38) mice, β-cell proliferation is not expected to increase in K_{ATP}-GOF/GCK$^{+/-}$ mice since both increased glycolytic flux and membrane depolarization are absent. Intracellular glucose flux appears to also regulate proliferation and apoptosis in human β-cells (41), as individuals bearing an activating mutation in GCK demonstrate hyperplastic islets (42,43). Together, these findings are well aligned with postprandial glucose increasing metabolic rate and insulin secretion, with an unchanged mass, and with persistently elevated glucose tilting the balance to *1*) increased insulin secretion and proliferation or *2*) increased metabolic rate with decompensation and reduced β-cell mass. Thus, paradoxically, reduction of glucose metabolism emerges as a novel mechanism to enhance glucose sensing, improve β-cell function, and maintain β-cell insulin content and β-cell identity in diabetes. This has critical implications for the prevention of β-cell exhaustion and glucotoxicity in diabetes progression, and preservation of β-cell mass and function by reduction of glucose metabolism in mouse models of diabetes may be key to explaining beneficial effects of insulin therapy and tight glycemic control observed (20,33,34,44–46), at least in the early stages of T2D.

Horses for Courses: Differential Consequences of Decreased Glucose Metabolism in Various Forms of Diabetes

In addition to the effects of glucose metabolism in proliferation and apoptosis, Ha et al. (47) developed a mathematical model of diabetes pathogenesis supporting the idea that metabolism-induced stress triggers reduction of β-cell mass, especially when insulin secretion is reduced. Consistent with this, haploinsufficiency of GCK in the *db/db* mouse model of obesity/T2D decreased β-cell stress–related gene expression and mitochondrial damage and improved insulin content and β-cell mass and identity (48). This correlates with our observation of reduced oxidative stress, improved mature β-identity genes, and reduced dedifferentiation in K_{ATP}-GOF/GCK$^{+/-}$ mice with respect to K_{ATP}-GOF. In contrast, genetic reduction of GCK in Akita mice (49) further increased endoplasmic reticulum (ER) stress and expression of apoptotic genes (50). Importantly, the Akita mouse is a model of ER stress–induced diabetes, and hence, the discrepancy in the outcome of reduced glucose metabolism in this model versus K_{ATP}-GOF and *db/db* mice could arise from the distinctive underlying causes of the insulin deficiency. Thus, impaired β-cell growth/increased apoptosis in Akita mice (51), versus failure of glucose-dependent secretion in K_{ATP}-GOF mice (6,21) and potentially in *db/db* mice (40), could explain the differential outcomes by decreased β-cell glucose metabolism.

A balance between food intake and energy consumption is reflected in body weight. In contrast to the significant reduction of body weight, fat mass, and energy efficiency in K_{ATP}-GOF (even with increased food intake), K_{ATP}-GOF/GCK$^{+/-}$ mice maintained normal body weight, fat mass, and energy efficiency and had normal food intake and physical activity. The contribution of fat mass to energy expenditure is substantially greater than predicted from the metabolic cost of adipose tissue, and it is leptin dependent. In K_{ATP}-GOF mice, increased plasma glucagon and decreased leptin, both of which were normalized in K_{ATP}-GOF/GCK$^{+/-}$ mice, could therefore explain the significant increase in blood glucose and food intake. Several lines of evidence implicate a role of leptin in inhibiting glucagon secretion from pancreatic α-cells (52,53). Thus, we speculate that the increase in plasma leptin levels in K_{ATP}-GOF/GCK$^{+/-}$ mice will reduce glucagon secretion and plasma glucagon levels, which in turn will help to maintain body weight and adiposity and to restore physical activity and energy expenditure in these mice. Similar improvements in metabolic parameters were observed in *ob/ob* mice exposed to a ketogenic diet (54) and in K_{ATP}-GOF mice subjected to a high-fat diet (25), both interventions inducing reduction of β-cell glucose metabolism (55).

Systemic Consequences of Improved β-Cell Identity and Function

Maintenance of normal WAT and improvement of hepatic steatosis in K_{ATP}-GOF/GCK$^{+/-}$ mice is consistent with the idea that reducing β-cell glucotoxicity improves peripheral tissue mass and function and correlates with the increase in PPARα and amelioration of fatty liver observed in mice fed a high-fructose diet (56,57). On the other hand, BAT is recognized as the major site of sympathetically activated nonshivering thermogenesis during cold exposure and after spontaneous hyperphagia (58). Enlarged brown adipocytes with large unilocular vacuoles in K_{ATP}-GOF mice, but not in K_{ATP}-GOF/GCK$^{+/-}$ mice, suggests a BAT-to-WAT transition in the former. Transcriptional regulation of the Ucp-1 gene is controlled by regulatory elements critical for both white and brown fat adipogenesis, in agreement with our findings of decreased Ucp-1 and Pparα messages in K_{ATP}-GOF mice and their partial restoration in K_{ATP}-GOF/GCK$^{+/-}$ mice.

Although liver PPARγ contributes to hepatic steatosis and regulation of body fat mass, we did not see changes in either K_{ATP}-GOF or K_{ATP}-GOF/GCK$^{+/-}$ mice. Highlighting

the crucial role of liver PPARα for whole-body fatty acid homeostasis and protection against fatty liver (59), increased PPARα in K_{ATP}-GOF/$GCK^{+/-}$ mice correlated with hydrolysis of hepatic triglycerides and reduction in triglyceride content and with the effects observed in liver-specific PPARα knockout mice (60). Reduced FAS in livers of K_{ATP}-GOF mice suggest that fat accumulation is promoted by peripheral lipolysis rather than increased liver lipogenesis. Liver-specific FAS knockout mice showed fatty liver upon high-carbohydrate diet feeding potentially because of increased hepatic malonyl-CoA, which will inhibit fatty acid β-oxidation (61). On the other hand, increased ATGL and HSL in livers of K_{ATP}-GOF/$GCK^{+/-}$ is consistent with decreased liver fat and increased β-oxidation, correlating with amelioration of hepatic steatosis and improvement of liver function in *ob/ob* mice and in high-fat diet–induced obesity ATGL- and HSL-overexpressing mice (29).

Conclusions

We demonstrate that reduction of β-cell glucose metabolism protects against reduction of insulin content and loss of β-cell identity and dedifferentiation in a K_{ATP}-GOF model of neonatal diabetes (Fig. 6). By extrapolation to findings in other forms of diabetes that result from failure of glucose-dependent insulin secretion, reduced glucose metabolism paradoxically emerges as a mechanism to prevent glucotoxicity-induced loss of functional β-cell mass in diabetes and to maintain adipose tissue and liver function, as well as metabolic parameters.

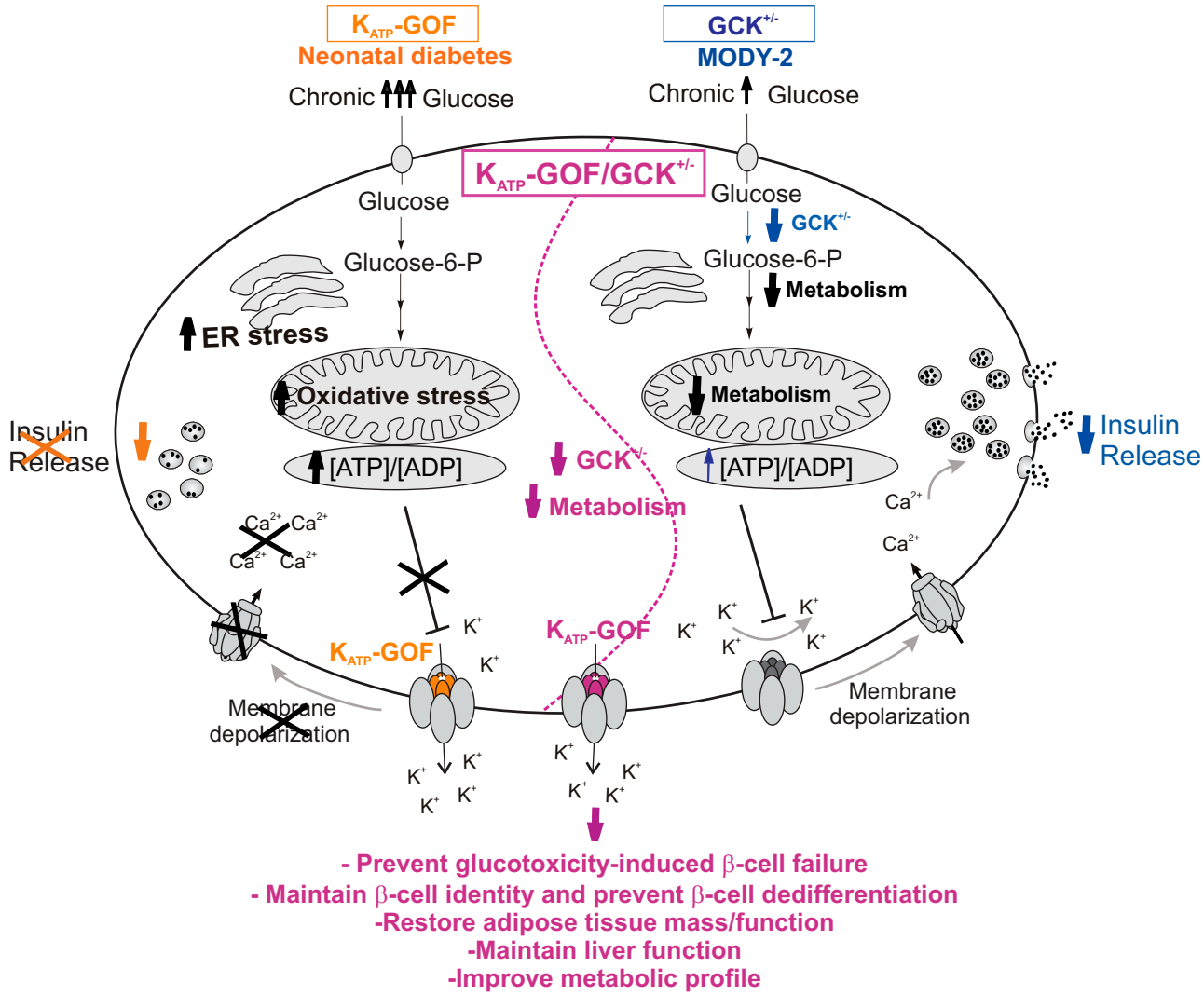

Figure 6—Schematic representation of the glucose metabolism and insulin secretory pathway in a pancreatic β-cell: *1*) mice with β-cell–specific K_{ATP}-GOF mutation (orange, left side of the cell); *2*) mice with β-cell–specific $GCK^{+/-}$ haploinsufficiency (blue, right side of the cell), and *3*) a combination of both β-cell–specific K_{ATP}-GOF and $GCK^{+/-}$ (purple, middle of the cell). MODY-2, maturity-onset diabetes of the young 2.

Funding. This work was supported by National Institutes of Health grants R01DK098584 and R01DK123163 (to M.S.R.). The authors also acknowledge the Diabetes Models Phenotyping Core and the Metabolic Tissue Function Core, Diabetes Research Center, Washington University in St Louis, MO, National Institutes of Health grant P30 DK020579.
The funders had no role in the study design, data collection and analysis, decision to publish, or preparation of the manuscript.
Duality of Interest. No potential conflicts of interest relevant to this article were reported.
Author Contributions. Z.Y., M.Fo., Z.A.S., A.L.C., M.Fu., and M.S.R. performed the experiments and data analysis. Z.Y. and M.S.R. wrote the manuscript. C.G.N. and M.S.R. conceptualized the study and edited the manuscript. All authors read and approved the final version of the manuscript. M.S.R. is the guarantor of this work and, as such, had full access to all the data in the study and takes responsibility for the integrity of the data and the accuracy of the data analysis.
Prior Presentation. Parts of this study were presented in oral form at the 78th Scientific Sessions of the American Diabetes Association, 22–26 June 2018.

References

1. Eizirik DL, Pasquali L, Cnop M. Pancreatic β-cells in type 1 and type 2 diabetes mellitus: different pathways to failure. Nat Rev Endocrinol 2020; 16:349–362
2. Gloyn AL, Pearson ER, Antcliff JF, et al. Activating mutations in the gene encoding the ATP-sensitive potassium-channel subunit Kir6.2 and permanent neonatal diabetes. N Engl J Med 2004;350:1838–1849
3. Flanagan SE, Clauin S, Bellanné-Chantelot C, et al. Update of mutations in the genes encoding the pancreatic beta-cell K(ATP) channel subunits Kir6.2 (KCNJ11) and sulfonylurea receptor 1 (ABCC8) in diabetes mellitus and hyperinsulinism. Hum Mutat 2009;30:170–180
4. Nielsen EM, Hansen L, Carstensen B, et al. The E23K variant of Kir6.2 associates with impaired post-OGTT serum insulin response and increased risk of type 2 diabetes. Diabetes 2003;52:573–577
5. Koster JC, Marshall BA, Ensor N, Corbett JA, Nichols CG. Targeted overactivity of beta cell K(ATP) channels induces profound neonatal diabetes. Cell 2000;100:645–654
6. Remedi MS, Kurata HT, Scott A, et al. Secondary consequences of beta cell inexcitability: identification and prevention in a murine model of K(ATP)-induced neonatal diabetes mellitus. Cell Metab 2009;9:140–151
7. Remedi MS, Agapova SE, Vyas AK, Hruz PW, Nichols CG. Acute sulfonylurea therapy at disease onset can cause permanent remission of KATP-induced diabetes. Diabetes 2011;60:2515–2522
8. Wang Z, York NW, Nichols CG, Remedi MS. Pancreatic β cell dedifferentiation in diabetes and redifferentiation following insulin therapy. Cell Metab 2014;19:872–882
9. Bensellam M, Jonas JC, Laybutt DR. Mechanisms of β-cell dedifferentiation in diabetes: recent findings and future research directions. J Endocrinol 2018;236:R109–R143
10. Butler AE, Janson J, Bonner-Weir S, Ritzel R, Rizza RA, Butler PC. Beta-cell deficit and increased beta-cell apoptosis in humans with type 2 diabetes. Diabetes 2003;52:102–110
11. Cinti F, Bouchi R, Kim-Muller JY, et al. Evidence of β-cell dedifferentiation in human type 2 diabetes. J Clin Endocrinol Metab 2016;101:1044–1054
12. Guo S, Dai C, Guo M, et al. Inactivation of specific β cell transcription factors in type 2 diabetes. J Clin Invest 2013;123:3305–3316
13. Moin ASM, Butler AE. Alterations in beta cell identity in type 1 and type 2 diabetes. Curr Diab Rep 2019;19:83
14. Matschinsky F, Liang Y, Kesavan P, et al. Glucokinase as pancreatic beta cell glucose sensor and diabetes gene. J Clin Invest 1993;92:2092–2098
15. Magnuson MA, She P, Shiota M. Gene-altered mice and metabolic flux control. J Biol Chem 2003;278:32485–32488
16. Chen C, Hosokawa H, Bumbalo LM, Leahy JL. Mechanism of compensatory hyperinsulinemia in normoglycemic insulin-resistant spontaneously hypertensive rats. Augmented enzymatic activity of glucokinase in beta-cells. J Clin Invest 1994;94:399–404
17. Liang Y, Najafi H, Matschinsky FM. Glucose regulates glucokinase activity in cultured islets from rat pancreas. J Biol Chem 1990;265:16863–16866
18. Talchai C, Xuan S, Lin HV, Sussel L, Accili D. Pancreatic β cell dedifferentiation as a mechanism of diabetic β cell failure. Cell 2012;150:1223–1234
19. Robertson RP, Harmon J, Tran PO, Poitout V. Beta-cell glucose toxicity, lipotoxicity, and chronic oxidative stress in type 2 diabetes. Diabetes 2004; 53(Suppl. 1):S119–S124
20. Wajchenberg BL. Beta-cell failure in diabetes and preservation by clinical treatment. Endocr Rev 2007;28:187–218
21. Benninger RK, Remedi MS, Head WS, Ustione A, Piston DW, Nichols CG. Defects in beta cell Ca^{2+} signalling, glucose metabolism and insulin secretion in a murine model of K(ATP) channel-induced neonatal diabetes mellitus. Diabetologia 2011;54:1087–1097
22. Terauchi Y, Sakura H, Yasuda K, et al. Pancreatic beta-cell-specific targeted disruption of glucokinase gene. Diabetes mellitus due to defective insulin secretion to glucose. J Biol Chem 1995;270:30253–30256
23. Remedi MS, Koster JC, Patton BL, Nichols CG. ATP-sensitive $K+$ channel signaling in glucokinase-deficient diabetes. Diabetes 2005;54:2925–2931
24. Emfinger CH, Yan Z, Welscher A, et al. Contribution of systemic inflammation to permanence of K_{ATP}-induced neonatal diabetes in mice. Am J Physiol Endocrinol Metab 2018;315:E1121–E1132
25. Yan Z, Shyr ZA, Fortunato M, et al. High-fat-diet-induced remission of diabetes in a subset of K_{ATP} -GOF insulin-secretory-deficient mice. Diabetes Obes Metab 2018;20:2574–2584
26. Yasuhara D, Naruo T, Nagai N, Tanaka M, Muranaga T, Nozoe S. Insulinogenic index at 15 min as a marker of nutritional rehabilitation in anorexia nervosa. Am J Clin Nutr 2003;77:292–299
27. Shyr ZA, Wang Z, York NW, Nichols CG, Remedi MS. The role of membrane excitability in pancreatic β-cell glucotoxicity. Sci Rep 2019;9:6952
28. Lodhi IJ, Dean JM, He A, et al. PexRAP Inhibits PRDM16-Mediated Thermogenic Gene Expression. Cell Rep 2017;20:2766–2774
29. Reid BN, Ables GP, Otlivanchik OA, et al. Hepatic overexpression of hormone-sensitive lipase and adipose triglyceride lipase promotes fatty acid oxidation, stimulates direct release of free fatty acids, and ameliorates steatosis. J Biol Chem 2008;283:13087–13099
30. Kim-Muller JY, Zhao S, Srivastava S, et al. Metabolic inflexibility impairs insulin secretion and results in MODY-like diabetes in triple FoxO-deficient mice. Cell Metab 2014;20:593–602
31. Jonas JC, Bensellam M, Duprez J, Elouil H, Guiot Y, Pascal SM. Glucose regulation of islet stress responses and beta-cell failure in type 2 diabetes. Diabetes Obes Metab 2009;11(Suppl. 4):65–81
32. Brereton MF, Iberl M, Shimomura K, et al. Reversible changes in pancreatic islet structure and function produced by elevated blood glucose. Nat Commun 2014;5:4639
33. Weng J, Li Y, Xu W, et al. Effect of intensive insulin therapy on beta-cell function and glycaemic control in patients with newly diagnosed type 2 diabetes: a multicentre randomised parallel-group trial. Lancet 2008;371:1753–1760
34. Torella R, Salvatore T, Cozzolino D, Giunta R, Quatraro A, Giugliano D. Restoration of sensitivity to sulfonylurea after strict glycaemic control with insulin in non-obese type 2 diabetic subjects. Diabete Metab 1991;17:443–447
35. Alvarsson M, Sundkvist G, Lager I, et al. Effects of insulin vs. glibenclamide in recently diagnosed patients with type 2 diabetes: a 4-year follow-up. Diabetes Obes Metab 2008;10:421–429
36. Greenwood RH, Mahler RF, Hales CN. Improvement in insulin secretion in diabetes after diazoxide. Lancet 1976;1:444–447
37. Qvigstad E, Kollind M, Grill V. Nine weeks of bedtime diazoxide is well tolerated and improves beta-cell function in subjects with type 2 diabetes. Diabet Med 2004;21:73–76

38. Porat S, Weinberg-Corem N, Tornovsky-Babaey S, et al. Control of pancreatic β cell regeneration by glucose metabolism. Cell Metab 2011;13: 440–449
39. Nichols CG, Remedi MS. The diabetic β-cell: hyperstimulated vs. hyperexcited. Diabetes Obes Metab 2012;14(Suppl. 3):129–135
40. Jahan I, Corbin KL, Bogart AM, et al. Reducing glucokinase activity restores endogenous pulsatility and enhances insulin secretion in islets from db/db mice. Endocrinology 2018;159:3747–3760
41. Kassem S, Bhandari S, Rodríguez-Bada P, et al. Large islets, beta-cell proliferation, and a glucokinase mutation. N Engl J Med 2010;362:1348–1350
42. Cuesta-Muñoz AL, Huopio H, Otonkoski T, et al. Severe persistent hyperinsulinemic hypoglycemia due to a de novo glucokinase mutation. Diabetes 2004;53:2164–2168
43. Kassem SA, Ariel I, Thornton PS, Scheimberg I, Glaser B. Beta-cell proliferation and apoptosis in the developing normal human pancreas and in hyperinsulinism of infancy. Diabetes 2000;49:1325–1333
44. UK Prospective Diabetes Study (UKPDS) Group. Intensive blood-glucose control with sulphonylureas or insulin compared with conventional treatment and risk of complications in patients with type 2 diabetes (UKPDS 33). Lancet 1998;352:837–853
45. Alvarsson M, Sundkvist G, Lager I, et al. Beneficial effects of insulin versus sulphonylurea on insulin secretion and metabolic control in recently diagnosed type 2 diabetic patients. Diabetes Care 2003;26:2231–2237
46. Ilkova H, Glaser B, Tunçkale A, Bagriaçik N, Cerasi E. Induction of long-term glycemic control in newly diagnosed type 2 diabetic patients by transient intensive insulin treatment. Diabetes Care 1997;20:1353–1356
47. Ha J, Satin LS, Sherman AS. A mathematical model of the pathogenesis, prevention, and reversal of type 2 diabetes. Endocrinology 2016; 157:624–635
48. Omori K, Nakamura A, Miyoshi H, et al. Glucokinase inactivation paradoxically ameliorates glucose intolerance by increasing β-cell mass in *db/db* mice. Diabetes 2021;70:917–931
49. Yoshioka M, Kayo T, Ikeda T, Koizumi A. A novel locus, Mody4, distal to D7Mit189 on chromosome 7 determines early-onset NIDDM in nonobese C57BL/6 (Akita) mutant mice. Diabetes 1997;46:887–894
50. Shirakawa J, Togashi Y, Sakamoto E, et al. Glucokinase activation ameliorates ER stress-induced apoptosis in pancreatic β-cells. Diabetes 2013;62:3448–3458
51. Riahi Y, Israeli T, Yeroslaviz R, et al. Inhibition of mTORC1 by ER stress impairs neonatal β-cell expansion and predisposes to diabetes in the *Akita* mouse. eLife 2018;7:e38472
52. Denroche HC, Huynh FK, Kieffer TJ. The role of leptin in glucose homeostasis. J Diabetes Investig 2012;3:115–129
53. Tudurí E, Marroquí L, Soriano S, et al. Inhibitory effects of leptin on pancreatic alpha-cell function. Diabetes 2009;58:1616–1624
54. Badman MK, Kennedy AR, Adams AC, Pissios P, Maratos-Flier E. A very low carbohydrate ketogenic diet improves glucose tolerance in ob/ob mice independently of weight loss. Am J Physiol Endocrinol Metab 2009;297: E1197–E1204
55. Lu B, Kurmi K, Munoz-Gomez M, et al. Impaired β-cell glucokinase as an underlying mechanism in diet-induced diabetes. Dis Model Mech 2018;11: dmm033316
56. Chan SM, Sun RQ, Zeng XY, et al. Activation of PPARα ameliorates hepatic insulin resistance and steatosis in high fructose-fed mice despite increased endoplasmic reticulum stress. Diabetes 2013;62:2095–2105
57. Ip E, Farrell GC, Robertson G, Hall P, Kirsch R, Leclercq I. Central role of PPARalpha-dependent hepatic lipid turnover in dietary steatohepatitis in mice. Hepatology 2003;38:123–132
58. Saito M, Matsushita M, Yoneshiro T, Okamatsu-Ogura Y. Brown adipose tissue, diet-induced thermogenesis, and thermogenic food ingredients: from mice to men. Front Endocrinol (Lausanne) 2020;11:222
59. Sapiro JM, Mashek MT, Greenberg AS, Mashek DG. Hepatic triacylglycerol hydrolysis regulates peroxisome proliferator-activated receptor alpha activity. J Lipid Res 2009;50:1621–1629
60. Montagner A, Polizzi A, Fouché E, et al. Liver PPARα is crucial for whole-body fatty acid homeostasis and is protective against NAFLD. Gut 2016;65: 1202–1214
61. Chakravarthy MV, Pan Z, Zhu Y, et al. "New" hepatic fat activates PPARalpha to maintain glucose, lipid, and cholesterol homeostasis. Cell Metab 2005;1:309–322